Snapshot Array Design Considerations for Rotorcraft Noise Characterization

Mary L. Houston
NASA Langley Research Center
Hampton, VA, USA

James H. Stephenson
U.S. Army Combat Capabilities Development Command
Aviation & Missile Center
Hampton, VA, USA

Kyle A. Pascioni Colin M. Stutz
NASA Langley Research Center
Hampton, VA, USA

ABSTRACT

Acoustic flight testing of rotorcraft often involves generating noise source hemispheres to gain an understanding about the aircraft's acoustic emissions. However, aerodynamically complex Urban Air Mobility and Future Vertical Lift vehicles may not maintain a steady aerodynamic state during flight, making source hemispheres measured using traditional linear arrays unreliable or difficult to interpret. To address this challenge, all emission angles need to be measured simultaneously. This has lead to the concept of the two dimensional 'snapshot' array layout. A mathematically defined microphone distribution was utilized to achieve uniform coverage on the source hemisphere. Within the chosen distribution, two lower microphone count distributions are embedded, allowing for a comparison of the effects of number of microphones. The array was deployed as part of a joint Army/NASA acoustic research flight test in July of 2024. Data were collected using an MD530F helicopter as the test vehicle, executing both steady and unsteady flight. Analysis of the array resolution is used to determine adequate channel count and spatially varying sensitivity to array density.

INTRODUCTION

Acoustic hemispheres have long been used to characterize the directivity of rotorcraft noise (Ref. 1). In the past, this has meant having the aircraft maintain a constant aerodynamic state while flying over a linear array of ground-based microphones so that acoustic measurements may be taken at different emission angles. For conventional helicopters, this can be achieved by maintaining a steady flight condition, as is described in numerous publications including Refs. 2 and 3. Aerodynamically complex multirotor Urban Air Mobility (UAM) or Future Vertical Lift (FVL) vehicles may present challenges to accurately measure because they do not necessarily maintain a steady aerodynamic state, even with constant airspeed. Additionally, the numerous independently controlled propulsors, which are a feature of many UAM vehicle designs, allow for non-unique trim states for the same operating condition. This is demonstrated in data acquired from the Joby Aviation preproduction prototype data found in Ref. 4.

To address this challenge, all directivity angles need to be measured simultaneously to "freeze" the aircraft state and collect data over the full hemisphere in a near instant in time, as was done in Refs. 5 and 6. If the aircraft state is known, these hemispheres can more accurately portray directivity characteristics and also serve as more reliable validation data for prediction tools. This need has lead to the development of the two-dimensional 'snapshot' array. An early version of this array type was deployed during a flight test in 2022 as described in Ref. 7. That specific array had 21 microphones, the locations of which were selected manually by the test engineer based on testing experience and presumed data needs. Upon processing the results, it was unclear if that array configuration provided sufficient angular resolution to capture the acoustic directivity. Further investigation has lead to leveraging mathematically defined point distribution schemes to get even coverage for varying numbers of channels. While a high channel count might improve data quality through greater resolution, the array pattern is limited by the number of available recording systems and personnel to deploy them.

Determining an adequate channel count was one goal of this research effort. A desirable array layout would be one for which evenly distributed low channel count arrays can be selected out of an evenly distributed high channel count array, allowing the researchers to assess the impacts of varied channel count without the necessity of deploying multiple configurations. A distribution scheme based on Lebedev quadrature (Ref. 8) was found to meet the requirements of even coverage,

The Vertical Flight Society's 81st Annual Forum and Technology Display, Virginia Beach, USA, May 20-22, 2025.

equipment availability, and the lower channel count embedded arrays. Herein, array resolution studies are conducted. Two methods are employed: first Leave One Out Cross Validation (LOO-CV) is carried out to to identify regions of sensitivity in the distributions (Ref. 9). Second, image processing methods such as the Structural Similarity Index Measure (SSIM) (Ref. 10), or simply taking the Absolute Difference (AD) in levels, are conducted to compliment the LOO-CV. The advantage of LOO-CV is that it does not require a reference image like AD and SSIM, the disadvantage is that it is computationally more intensive.

POINT DISTRIBUTION SCHEMES

Geodesic and Lebedev quadrature-based distribution schemes were considered. Both schemes result in regular and symmetrical distribution of points on the surface of a sphere, but only certain numbers of loci are possible. The geodesic distribution provides more uniform coverage of the surface, but the Lebedev distribution has a greater number of allowable point counts.

A Lebedev distribution was selected resulting in a 61-point array on the lower hemisphere. Upon selection, the actual microphone locations were judiciously modified to meet experimental constraints, specific research needs, and equipment availability. First, the points were shifted toward the center such that there were no points within 10° of the horizon plane. This was done to ensure that the distribution was physically realizable when projected to the ground. This initial distribution is shown by the orange circles in Figure 1a. Next, 12 microphones were added at 7.5° from the horizon, the black squares in Figure 1a, to increase data resolution in that region, as that is an area of importance to the research goals. Finally, six more microphones, the green squares in Figure 1a, were placed near the center of the array where the slew rate is high during flyover. Hemispheres are displayed using the Lambert projection such that 0° azimuth is aligned with the tail of the vehicle and 180° is aligned with the nose. Elevation is such that −90° is directly below the vehicle and 0° is the horizon of the hemisphere. For conventional helicopters the horizon is defined by the rotor plane. Projecting this distribution to a ground plane from a distance of 61 m (200 ft) results in a symmetric two-dimensional circular array of microphones with a diameter of approximately 926 m (3040 ft), as seen in Figure 1b.

One of the research objectives of this work was to determine the appropriate array resolution given the constraints on equipment availability, cost, and personnel, all of which limit the achievable channel count. It was found that a 25-element Lebedev distribution is almost perfectly represented in the selected 61-element distribution, as seen in Figure 2, with deviation being $\mathcal{O}(1^\circ)$. This convenient feature will allow a resolution study to be conducted to determine if the improvements gained from the higher channel count are worth the effort to

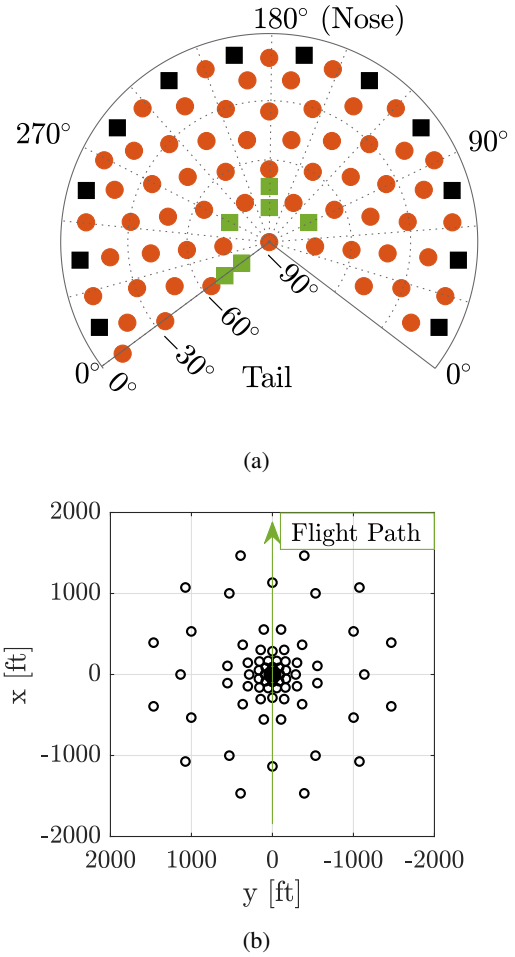

Figure 1: (a) Factor eight Lebedev distribution (orange circles) with addition of microphones to horizon (black squares) and underneath (green squares). (b) Array projected onto ground plane.

deploy the additional equipment. Because the distributions do not precisely overlap at all points, the average values of the near-overlapping locations were taken.

A third distribution can be found by removing the 25-element distribution from the 61-element distribution. This leaves a 36-element array with regularly distributed microphones, the orange circles not co-located with blue diamonds in Figure 2. The addition of the 12 microphones to the outer perimeter (black squares in Figure 1a), brings the number of unique distributions to six: 25 elements, 37 elements, 36 elements, 48 elements, 61 elements and 73 elements. Properties of these six arrays will be explored in the *Resolution Study* subsection. The six additional microphones placed at the center of the array (green squares in Figure 1a) for for the 79-element array were found to have a negligible effect on resolution. However, this array will be used as a reference case for some comparisons.

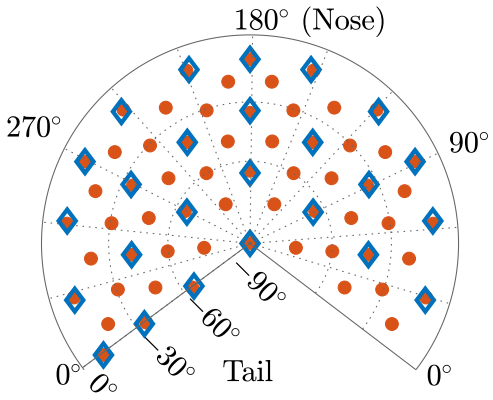

Figure 2: Two overlapping Lebedev distributions: 25 elements and 61 elements.

FIELD DEPLOYMENT

The resulting two-dimensional microphone array as deployed is shown in Figure 3. Some adjustments in microphone location were made to accommodate constraints of the test site - specifically plant life growing in some of the desired locations and unexpected restricted access to the southern part of the array. The latter adjustment resulted in microphones 6 and 7 being shifted northward by ≈ 6 m. The microphones are numbered sequentially working counter-clockwise and outside-in such that microphone 79 is at the center of the array and defines the origin of the coordinate system. This coordinate system is defined such that the primary flight track is in the positive X-direction, the positive Y-direction is to the vehicle's port (left) and positive Z-direction is up.

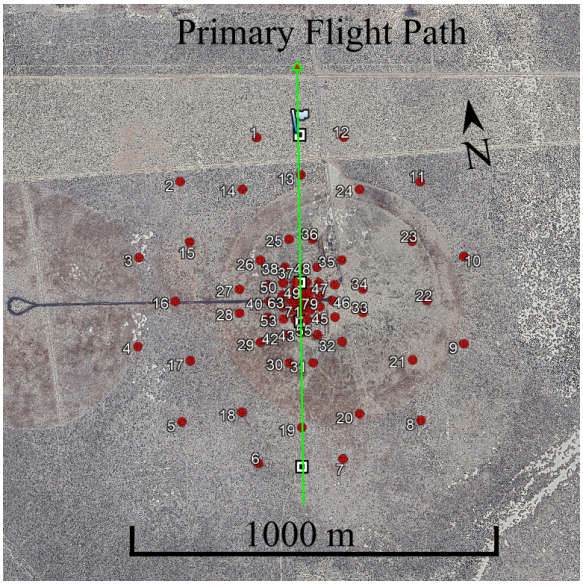

Figure 3: Snapshot microphone array deployed at the test site.

The deployed Wireless Acoustic Measurement System (WAMS II) utilizes 400 mm ground boards with microphones offset to minimize edge effects (Ref. 11). For this test, the ground boards were rotated such that the bulk of the board was directed toward the center of the array to minimize ground effects at grazing angles of incidence. Data are sampled simultaneously at 50 kHz and 24-bit resolution for all 79 recording stations. GPS timing is used to maintain synchronization. A detailed description of a single recording station can be found in Ref. 12. The acoustic data are then paired with aircraft GPS tracking data to identify the observer angles of the moving vehicle. The vehicle position is provided by the second generation Aircraft Navigation and Tracking System (ANTS2) with measurement being recorded in UTC. Position is relative to the center of the microphone array. Flights executed over this array included both aerodynamically steady and unsteady maneuvers. Details on maneuvering flight can be found in Ref. 13, and an overview of the test may be found in Ref. 12.

NOISE HEMISPHERE CREATION

As explained in the previous section, the microphone locations were chosen such that they would provide reasonably even coverage when projected to a noise hemisphere virtually surrounding the aircraft. This section will focus on the methodology employed for the creation of the snapshot hemisphere. For creation of a flyover hemisphere using a linear microphone array, the reader is referred to Ref. 1.

Acoustic Depropagation

The snapshot hemisphere is made using the half-second of data centered at the time when the vehicle passes over the center of the array. Vehicle tracking data are interpolated to find both the Y and Z coordinates and the source time for which $X = 0$, defined as X_0, Y_0, Z_0, τ_0 such that $X_0(\tau_0) = 0$.

Using these coordinates, the distances between the vehicle and the microphone locations are calculated. Microphone locations are designated as X_i, Y_i, Z_i, where $i = 1 : n_{mics}$ is the microphone index. Ground weather stations embedded in the array measure the air temperature, pressure, and relative humidity during testing. The weather data are used to calculate the speed of sound and hence transmission time for the emissions from the source to reach the microphones. The time when the acoustic signal is emitted by the source is designated τ_0, and the time that the signal reaches microphone receiver location i is designated $t_{i,0}$. The distances involved are relatively short, ≈ 91 m to 457 m, so straight-line propagation is used.

A half-second segment of the pressure time history (PTH) is taken for each microphone, centered around $t_{i,0}$ such that $(t_{i,0} - 0.25 \leq t_{i,0} \leq t_{i,0} + 0.25)$ s. Pressure time histories were sampled at 50 kHz, so interpolation to the exact arrival time was not necessary. Acoustic spectral estimates are computed

using Welch's method with a Hamming window and 50% overlap. These estimates are then converted to sound pressure levels in units of dB relative to 20 μ Pa.

The sound pressure spectrum at each microphone is then back propagated to the surface of the hemisphere following:

$$SPL_{hemi} = SPL_{mic} + A_{spread} + A_{atm} + A_{ground}, \qquad (1)$$

where SPL_{mic} is the spectrum as measured by the microphone, A_{spread} is the amplitude loss due to spherical spreading, A_{atm} is the amplitude lost to atmospheric absorption, and A_{ground} is the effect of complex ground impedance. Atmospheric absorption takes the form of a frequency-dependent coefficient giving absorption per unit length, multiplied by the propagation distance, and is modeled following Ref. 14. Because the signal is being propagated back from the receiver to the source, both A_{spread} and A_{atm} have positive values. The use of acoustically hard ground boards allows ground impedance to be modeled as simple pressure doubling: $A_{ground} = -6.02$ dB.

Special Treatment for High Frequency Atmospheric Losses Near Horizon Plane

The atmospheric absorption model used predicts increased attenuation of high frequencies, especially in dry air. This can pose a problem when the levels added back are greater than the original signal, resulting in artificially high-amplitude high-frequency noise occurring near the horizon plane where the propagation distance is the longest. Figure 4 shows the expected attenuation of a 3 kHz signal over 457 m as a function of temperature and relative humidity. The white dots in this figure represent the measured atmospheric conditions for individual data runs. It can be seen that several runs are modeled as having excess of 20 dB attenuation. To mitigate this effect, each spectrum is compared to an ambient spectrum taken at a similar time of day. Starting at 250 Hz, the microphone spectrum is compared to the ambient spectrum, which has been increased by a constant six decibels. The frequency at which the microphone spectrum and the modified ambient spectrum intersect is saved, and A_{atm} is set to zero for all frequencies above that cutoff point. Six decibels are added to ensure the cutoff occurs when the signal has twice the sound pressure level of the background noise. Low or negative signal-to-noise ratio data are still back propagated using this method and spherical spreading is accounted for. An example of this can be seen in Figure 5, where the cutoff point is depicted by the dashed line around 2 kHz. Fortunately, high-frequency content is most prevalent below the aircraft, and so not at large propagation distances corresponding to angles near the horizon (Ref. 15). Thus, this modification only improves the hemisphere accuracy, particularly when viewing OASPL or other integrated metrics.

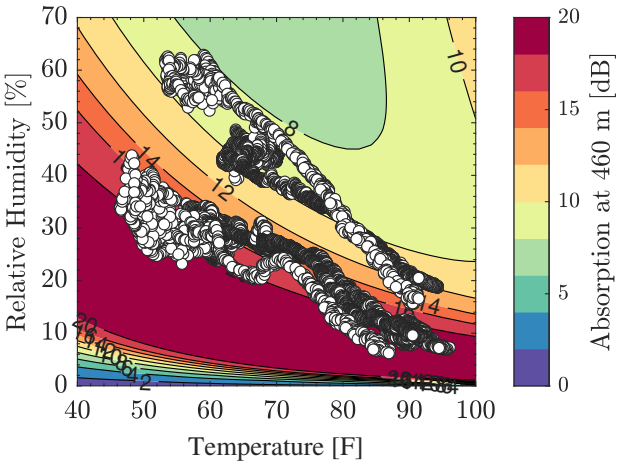

Figure 4: Atmospheric attenuation as a function of temperature and relative humidity for 3 kHz over a distance of ~460 m.

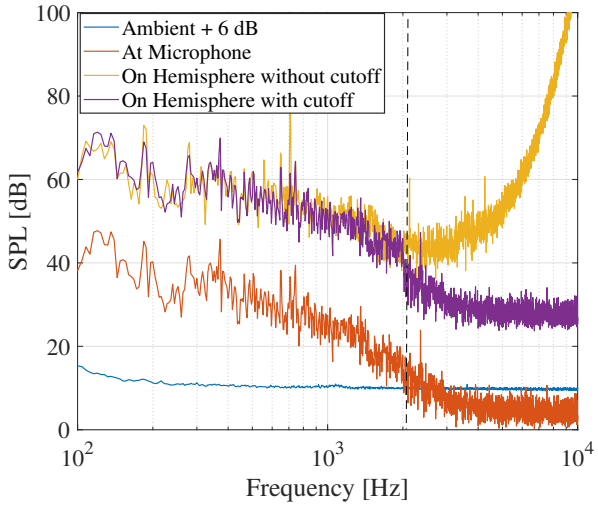

Figure 5: Determination of frequency cutoff point, above which atmospheric attenuation is over predicted

Interpolation of Data on the Hemisphere Surface

Acoustic data are stored in the form of spectra on the surface of a hemisphere of radius 30.48 m centered about the vehicle, typically at the main rotor hub for conventional helicopters. Data are stored at discrete locations on the surface. Depending on the final application, these locations can be the actual microphone locations as projected to the surface at the time of flyover, or the data can be interpolated onto a regular grid. The interpolation is done on the pressure-squared acoustic data for each frequency band using an inverse distance weighting scheme, described as *Modified Quadratic Shepard* in Ref. 16.

Interpolation to a regular grid is done to match the required

input format of a variety of land-use planning software, such as the Advanced Acoustic Model/ Rotorcraft Noise Model (Ref. 17). This format saves data onto a polar grid, where the parallels of latitude run from 0° at the nose of the aircraft to 180° at the tail in 5° increments. The lines of longitude run from −90° on the aircraft's port (left) side and +90° on the starboard (right) side, with the 0° line running from nose to tail below the aircraft in 5° increments. Files are typically saved in NetCDF format with accompanying meta-data as described in Ref 17.

RESULTS AND DISCUSSION

Initial investigation into the results is promising. Selected flight conditions are summarized in Table 1, where FPA stands for Flight Path Angle. Level and descending flights are used to demonstrate steady flight conditions. Noise hemispheres generated by the snapshot array and traditional linear array methods are compared. Condition codes and run numbers are provided in the table to assist the reader to cross-reference with other publications examining the same data set. At time of submission, this includes Refs. 13, 12, 18, and 19. Mathematical methods for assessing array resolution will be presented and applied to the data.

Table 1: Selected Flight Conditions

Condition Code	L3	D2
Run #	200175	200179
Description	Steady Level	Steady Descent
Speed [kts]	75	40
Entry Alt. [m]	61	100
FPA [deg.]	0	-3

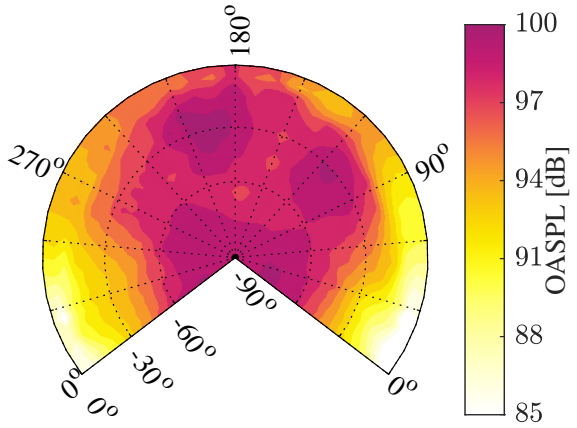

(a) Linear array

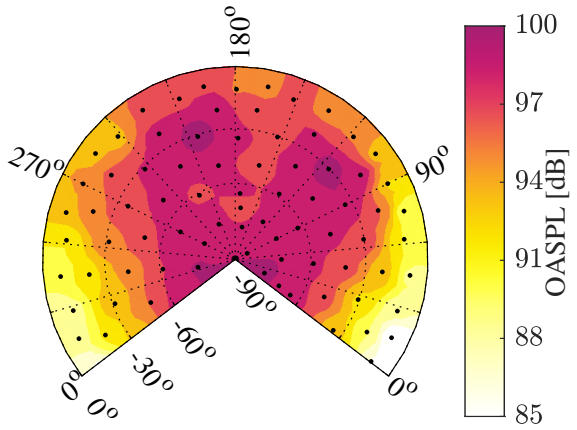

(b) Snapshot array

Figure 6: Variation in OASPL emissions from steady level flight condition at 75 kts. Hemispheres generated using (a) flyover method and (b) snapshot method.

Application to Steady Flights

Hemispheres made using the new snapshot array method are compared to those generated using the linear array method for the same flight conditions. Figures 6 and 7 both represent unweighted overall sound pressure level (OASPL) between 10 Hz and 5 kHz with a 15 dB dynamic range for a steady level flight and a steady descending flight, respectively. Both flights were executed early in the morning when both winds and thermal updrafts were negligible. In both figures, the hemisphere generated using the linear array method is shown first, followed by the same run processed using the new snapshot array method. It can be seen that the two figures are nearly identical, as expected for a steady flight condition in ideal weather conditions. The snapshot figures are generated using the full 79-microphone array with the black dots marking the microphone locations. The linear array figure was generated using a pseudo-linear array, this included microphones from the snapshot array distribution that were within 152 m of the x = 0 line. These results support both the utility of the flyover hemisphere for capturing steady flight and the equivalence of a high channel count snapshot array. The descending flight condition was included because it presented blade vortex interaction (BVI) noise, which often results in sharp, directive features. BVI noise is not usually present during level flight. Figure 7 demonstrates that this flight condition is likewise well accounted for using both the flyover and snapshot methods. The flyover array requires the vehicle to remain in steady flight for between 20 s to over one minute, depending on flight speed. The snapshot array, on the other hand, only requires the flight to remain steady for 0.5 s. Therefore, the snapshot array method is better suited than the linear array method for capturing unsteady flight conditions or conditions where the vehicle trim state is required to change to maintain a desired flight condition.

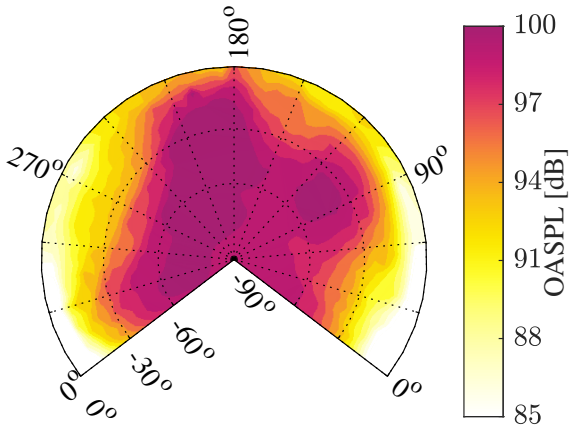

(a) Linear array

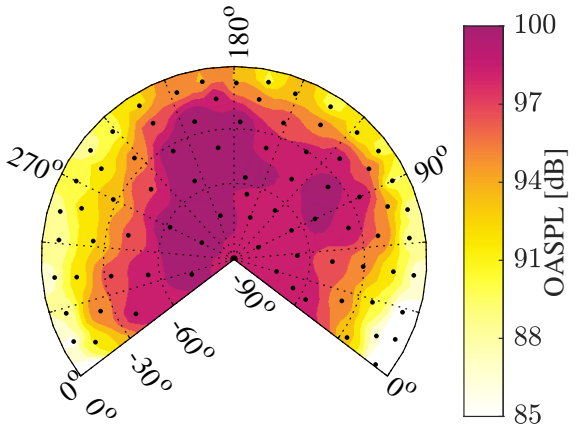

(b) Snapshot array

Figure 7: Variation in OASPL emissions from steady descending flight at 40 kts and -3° flight path angle. Hemispheres generated using (a) flyover method and (b) snapshot method.

Resolution Study

Measures of hemisphere coverage for the various microphone distributions must be estimated to investigate error as a function of resolution. Two measures of array resolution are defined: the distance from any given location on the hemisphere surface to the nearest available microphone location, or the number of microphone locations within a specified radius to any location on the hemisphere surface. It was found that the latter was better for identifying trends in error as a function of resolution, and so that definition is used in the evaluation.

Figure 8 shows the number of microphones within a radius of 30°, referred to as the Radius of Interpolation (ROI), of any point on the hemisphere surface. Note, these distributions represented the ideal case with precise microphone deployment and the vehicle centered above the array at an altitude of 61 m. The subfigures are arranged such that the addition of a horizon ring of 12 microphones to the arrays shown in the left column forms the arrays shown in the right column. For instance, the addition of the outer ring to the 25-microphone array, shown in Figure 8a, forms the 37-microphone array shown in Figure 8b. The ring of 12 microphones was added to improve resolution near the horizon, which is an important region to capture to meet research goals, but does not change coverage beneath the vehicle. For the lowest channel count array, 25 microphones, Figure 8a, there are areas in the array where only one microphone is in the RoI, meaning that only data from one point are used to estimate levels. In some instances for this distribution this coincides with microphone locations, in which case levels do not need to be estimated because they are directly measured. However, the horizon plane also shows sparse coverage. Consequently, values at that location are estimated through extrapolation from few available data points. Adding 12 horizon microphones, shown in Figure 8b, addressed coverage at the horizon, but there remain the interior locations with only information from one microphone.

For the intermediate channel count, 36 microphones shown in Figure 8c, coverage beneath the vehicle is improved. However, due to the manner in which this subarray was selected, there is poor coverage at the horizon, the nearest being at $\approx -20°$ instead of $-10°$. In this case adding the outer ring, forming the 48-element array shown in Figure 8d, increases the coverage in that area to at least two microphones. For the highest channel counts, 61- and 73- elements, Figures 8e and 8f show improved coverage across the horizon. The 61-element array has a minimal channel number at the horizon of three, which increases to four with the addition of the horizon ring. Mean, median, minimum and maximum number of microphones for all six distributions are provided in Table 2 for the 30° RoI. The impact of hemisphere resolution using these distributions is explored in the remainder of this section.

Table 2: Microphones within a radius of 30° for six-microphone distribution

Ch. Count	Ave	Med	Min	Max
25	2.8	3	1	4
37	4.1	4	1	6
36	3.9	4	1	8
48	5.3	5	2	8
61	6.7	7	3	12
73	8.0	8	4	17

Leave One Out Cross Validation Leave one out cross validation is a validation technique commonly used in machine learning. A data set is split into the training and testing sets, with the testing set containing only one entry. A model is built using the data in the training set and a response value is pre-

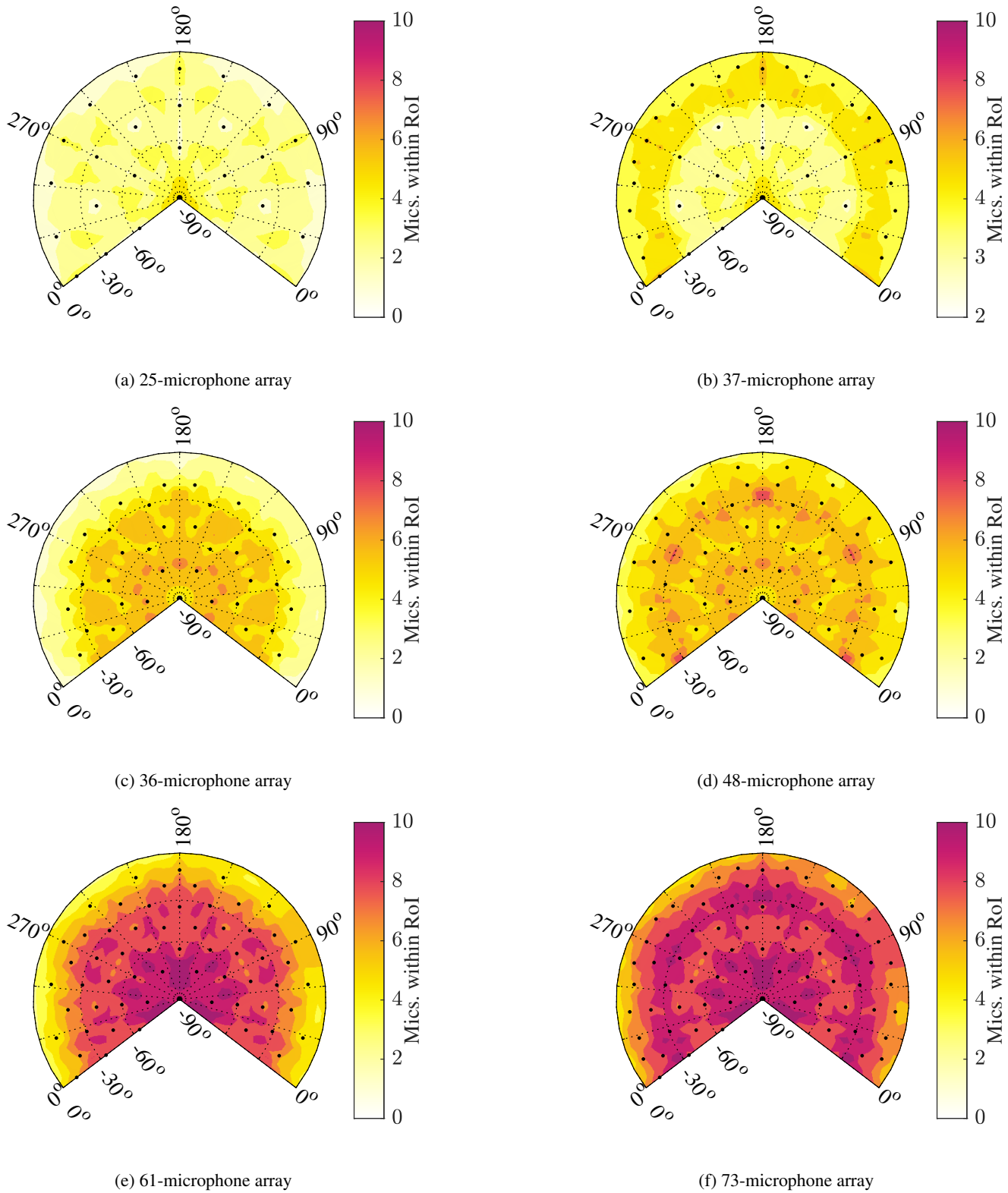

(a) 25-microphone array

(b) 37-microphone array

(c) 36-microphone array

(d) 48-microphone array

(e) 61-microphone array

(f) 73-microphone array

Figure 8: Available data points within a 30° radius of any location in the hemisphere surface.

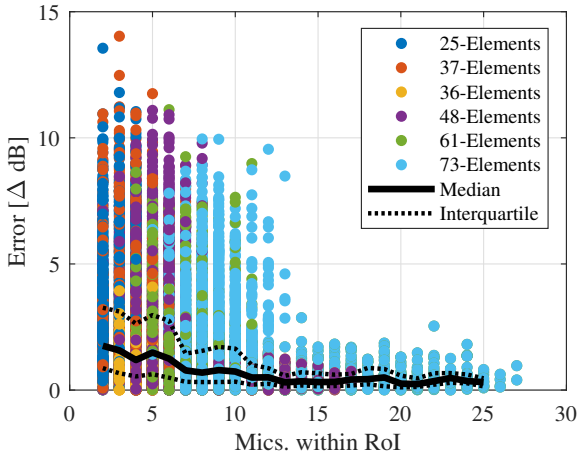

Figure 9: Error calculated by LOO-CV as a function of microphones within specific region of influence for all runs on day 200.

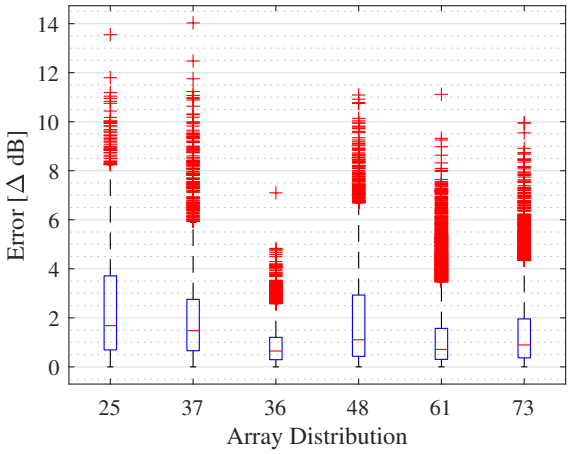

Figure 10: Data range by array. Left-to-right 25, 37, 36, 48, 61, and 73 elements

dicted for the one observation left out. The error can then be calculated by taking the difference between the prediction and the test data point. The process is repeated for all observations in the data set. For the present application, LOO-CV is used to identify regions on the hemisphere that are more sensitive to resolution as well as generally assess array resolution.

Rotorcraft noise can broadly be separated into main-rotor harmonic and high-frequency broadband components. Frequency ranges that will be explicitly discussed are the main-rotor blade passage frequency (MRBPF), nominally 40 Hz, so a frequency range of 36 Hz to 44 Hz is used to allow for variability in MRBPF; high-frequency broadband, or simply broadband (BB) noise, which is defined here to be 500 Hz to 5 kHz; as well as a full acoustic spectrum analyzed, defined here from 10 Hz to 5 kHz. This is done because rotor harmonic noise and BB typically have different directivity patterns (Ref. 15).

In this context, resolution is defined as the number of microphone locations within a specified radius from the omitted microphone location. Figure 9 shows point-by-point error as a function of the number of microphones within the RoI for the full frequency range, colored by which of the six array distributions is represented. Because this figure was generated using experimental data, the resolution value reached on the x-axis can be higher than those planned if the vehicle did not pass the array center at the prescribed altitude. It can be seen that there is a significant range in error values, particularly for low resolutions, where error ranges from almost zero to greater than 14 dB. This suggests that improved resolution resulting from increased channel counts acts to limit error. What is less obvious in this figure is the density of the error distribution, which is made more clear by addition of the overall median (solid line) and interquartile range (IQR, dashed lines). Therefore, the median error drops from 1.75 (IQR 0.87-3.26) dB for two microphones in the RoI, to 0.31 (IQR 0.14-0.46) dB for 25 microphones in the RoI. Due to the nature of LOO-CV, errors cannot be estimated for only one microphone in the RoI, so the x-axis starts at 2. Also, data points for resolutions greater than 25 microphones within the RoI are too sparse to be statistically reliable, for instance the columns for 26 and 27 have only 10 and 2 data points, respectively.

The impact of the specific distribution is displayed in Figure 10. Each box represents the overall error for each distribution. The center of the box represented the median value, the bottom and top of the box represent the 25^{th} and 75^{th} percentiles, respectively. The dashed line measures the range and the red crosses mark outliers. There may appear to be significant outliers, but bear in mind that the data are quite skewed and that each box represents thousands of data points. Considering the distributions again in pairs (25 and 37, 36 and 48, and 61 and 73) demonstrates two possible contributing factors to overall error. First, increasing channel count of the 25-element array to 37 elements decreases the median error, adding 12 horizon microphones reduces the median error from 1.68 (IQR 0.69-3.71) dB to 1.48 (IQR 0.66-2.75) dB.

However, the distribution of microphones near the horizon appears to have an unfavorable impact on the error when the initial array has higher density. This is especially clear considering the two middle boxes, representing the 36-element and 48-element arrays, which have median errors of 0.65 (IQR 0.29-1.21) dB and 1.11 (IQR 0.34-2.93) dB, respectively. Referring back to Figure 8c, one sees that the microphones are clustered toward the center for the 36-element array, reducing the spatial extent over which error can be evaluated. The addition of the outer ring of 12 significantly increases the area of coverage, enabling more complete accounting of error. This is a case where image processing methods do better because they consider all the spatial extent of the data, as will be discussed in the following section. It may also be related to the assump-

tions made around atmospheric attenuation in the vicinity of the horizon.

Finally, the addition of the outer ring has minimal impact when the channel count is high and already evenly distributed. However, it is still interesting to note that moving from the 61-microphone to 73-microphone element array does return a slightly higher median error and wider distribution, 0.71 (IQR 0.31-1.57) dB and 0.89 (IQR 0.36-1.96) dB, respectively. This again could be related to the greater total area considered in the calculations.

The range of error values witnessed when sorting both by RoI (Figure 9) or array channel count (Figure 10) necessitates inspecting the error distributions of the hemispheres directly. This is done in Figure 11 where the widest frequency range is presented. The left column shows the sounds pressure level contours for each distribution, while the right provides the error associated with that distribution. Again, it is most convenient to examine the error distributions in pairs. First, consider the acoustic hemispheres from the 25 and 37-element arrays, shown in Figures 11a and 11c, respectively. These SPL contours look largely identical apart from near the horizon where variation is noticeable. Considering the corresponding error contours, Figures 11b and 11d, we see that there is indeed improvement in the error about the horizon. However, the most prominent feature of these contours is the high level of error at the four microphone locations at $\approx -45^{\circ}$ elevation. As pointed out in describing Figures 8a and 8b, these are in fact areas with poor resolution, so estimated values at those locations draw from few and distant sources.

Now examining the 36- and 48- microphone distribution pair, with SPL contours shown in Figures 11e and 11g, respectively. The relatively tight clustering of the microphones in the 36-element array allows variation around the horizon to go unaccounted for, as can been seen in the corresponding error contour Figure 11f. Adding resolution to the horizon, as in the the 48-element array, allows this variation to be captured, which introduces the possibility for increased error to be measured, as is seen in Figure 11h. On the other hand, the tighter spacing of microphones near the center of both the 36- and 48-element arrays addresses the large error values present for the 25- and 37- element arrays.

Finally, consider the high channel count 61- and 73- element arrays, with SPL contours shown in Figures 11i and 11k, respectively. These appear practically identical. The most notable differences between Figures 11l and 11j, albeit still minor compared to the lower channel count arrays, appear near the horizon and demonstrate the improved accuracy in that region due to the additional channels.

As mentioned, the data were also split by frequency ranges, separating the MRBPF from BB noise. This shows the impact of different noise sources on error. For instance, Figure 12 shows the median and IQR for MRBPF and BB as a function of resolution, with the same values for the entire frequency range reproduced from Figure 9 for reference. Here, it is seen that both the MRBPF and BB sets have significantly higher levels of error for low resolution values, with levels becoming more equal for higher resolutions. Although it is slight, the MRBPF data set in particular shows higher error and greater uncertainty, as demonstrated by the IQR line, as compared to the BB data set.

Figure 13 shows the noise maps and error distribution in the MRBPF and BB frequency ranges from the 73-microphone distribution. It can be seen that the most significant error occurs to the rear of the aircraft near the horizon where the emitted noise level is minimal for any frequency range, enabling an over-prediction. This is not surprising given the challenges associated with capturing acoustic data at the horizon.

Image-Processing Methods Taking the absolute difference (AD) is the simplest way to compare array resolution. For this method, both hemispheres are interpolated onto a regular grid allowing for a point-by-point comparison to be made. The median of the point-by-point differences is a summary metric, where lower values indicate a better match. This method is simple to implement but requires a reference hemisphere. For this case, the reference hemisphere is a snapshot hemisphere made with the 79-point resolution, which analysis above shows is sufficient. This assumption is less than ideal because all subarrays are extracted from the 79-element array, but it is useful to demonstrate the effect of sparse coverage, particularly at the horizon plane, like in Figure 8c.

The SSIM is another pixel-by-pixel comparison method, however SSIM also incorporates inter-dependencies of pixels in the same region of the image as a method to capture differences in image structure. This method was explored to study array resolution but was found to yield results similar to the AD method.

Summary results of AD, as a function of channel count, can be see in Figure 14, where the black boxes, blue boxes and magenta boxes display the error distributions for the full frequency range, MRBPF range and BB range, respectively. The trend displayed generally indicates that increased channel count improves agreement to the reference hemisphere. This figure also demonstrates that neglecting regions of the hemisphere, as is the case for the 36-element array, leads to poor agreement. This is in contrast to the results from the LOO-CV analysis.

Absolute Difference also captures the variation in error presented by different frequency ranges. It can be seen that the MRBPF ranges and BB ranges have both greater median error and greater IQR than the full frequency range. This is expected since the greater frequency range over which SPL is integrated has the effect of evening spatial variations. Still, for all frequency ranges investigated, the overall trend of decreasing median error (apart from array 36) is observed. Additionally, MRBPF median error is is greater than BB median error

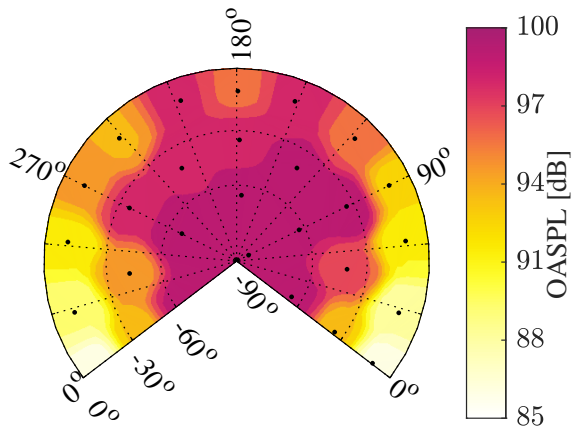

(a) 25-microphone array SPL

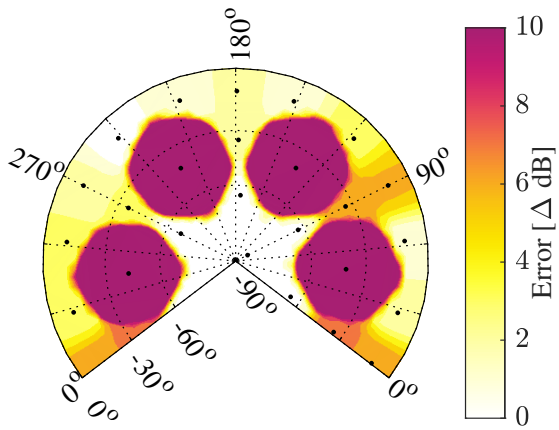

(b) 25-microphone array error

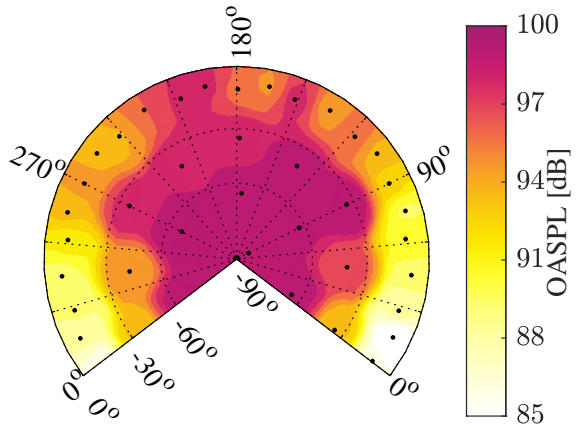

(c) 37-microphone array SPL

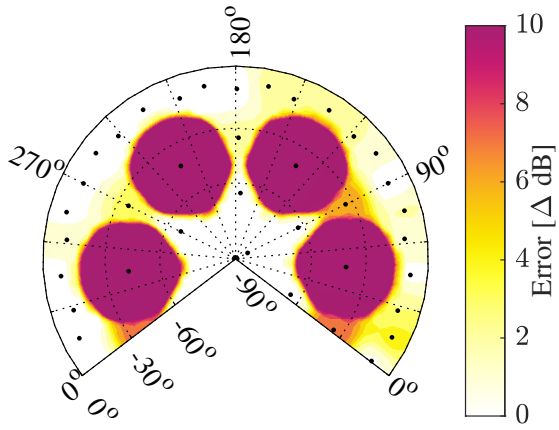

(d) 37-microphone array error

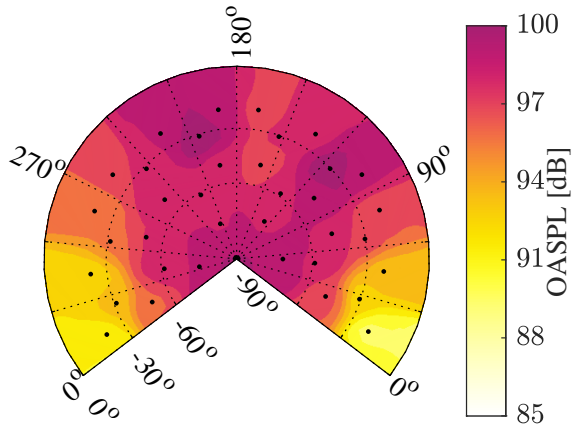

(e) 36-microphone array SPL

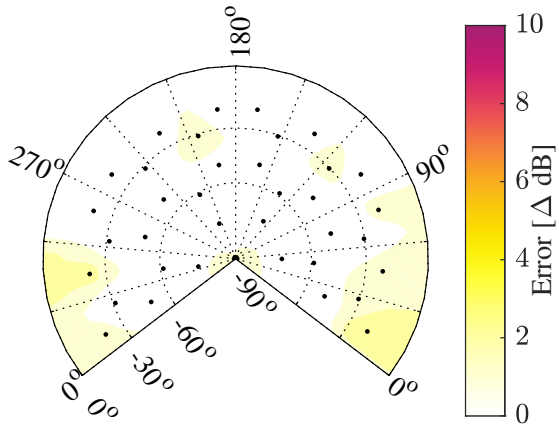

(f) 36-microphone array error

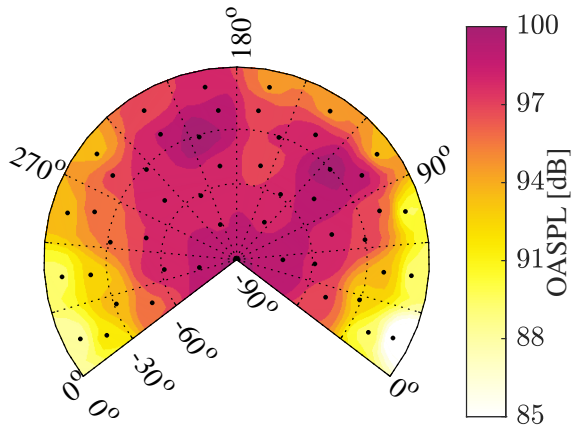

(g) 48-microphone array SPL

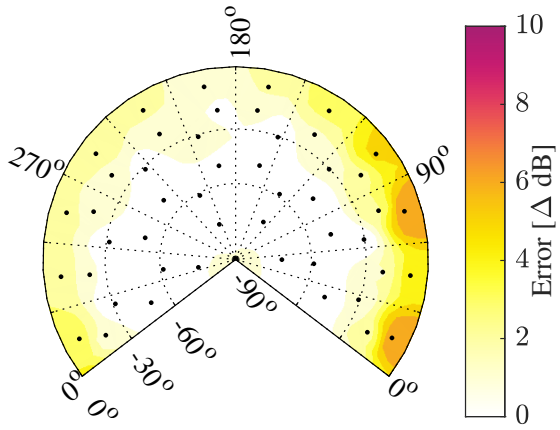

(h) 48-microphone array error

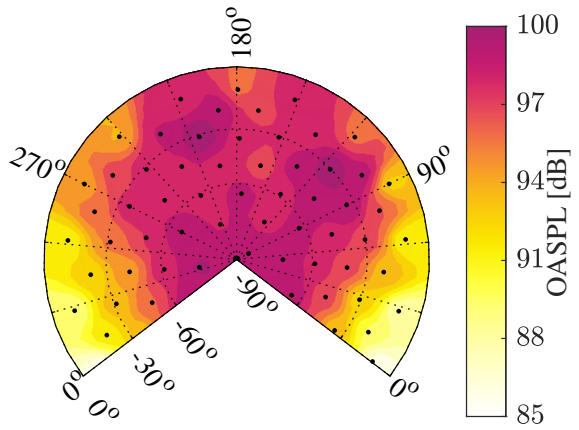

(i) 61-microphone array SPL

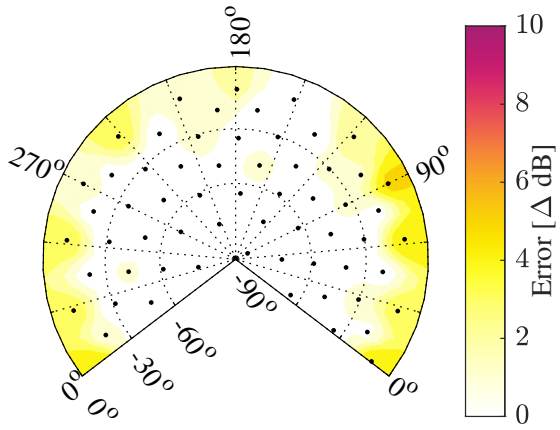

(j) 61-microphone array error

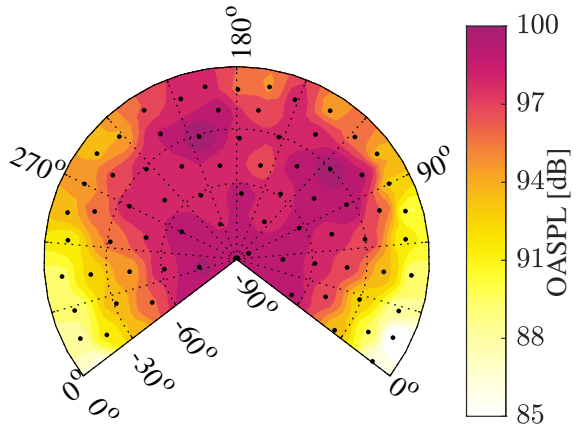

(k) 73-microphone array SPL

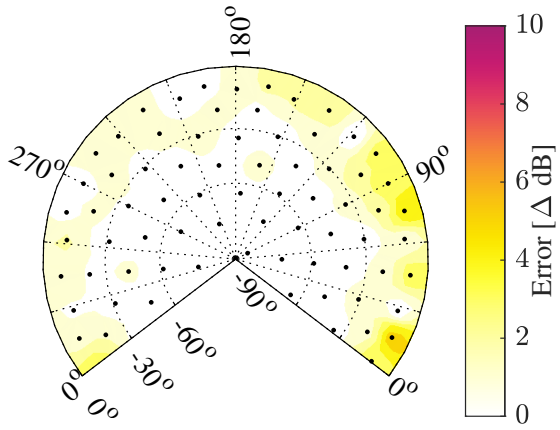

(l) 73-microphone array error

Figure 11: Contour plots and associated errors by channel count for for steady level flight at 75 kts.

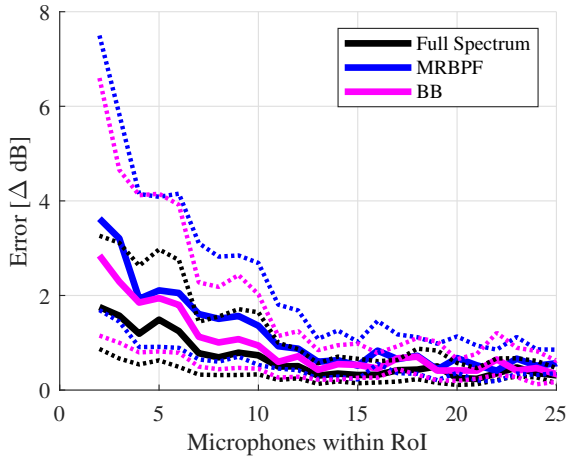

Figure 12: Summary median (solid line) and interquartile range (dashed) of all explored frequency ranges.

in all but the 25-element case. The greater median error and IQR for MRBPF was also observed in the LOO-CV results (Figure. 12).

Consider the AD error contours shown in Figure 15. Inspecting the first row representing the 25-element and 37-element arrays, Figures 15a and 15b, respectively, it can be seen that error levels and directivity patterns are similar, suggesting a similar level of overall error. As displayed by the corresponding black boxes in Figure 14, the median error values are 0.55 (IQR 0.23-1.22) dB and 0.37 (IQR 0.12-0.97) dB, for array distributions 25 and 37, respectively.

Moving to the second row, Figures 15c and 15d show the 36-element and 48-element arrays, respectively. In this case, the addition of the outer microphone ring significantly reduces error at the horizon and reduces the median error from 0.87 (IQR 0.14-2.34) dB to 0.25 (IQR 0.06-0.70) dB. This is in contrast to the increase in error as calculated using LOO-CV, indicating the importance of resolution near the horizon for predicting overall error trends.

Finally, we examine the third row where the 61- and 73- element array error distributions are presented. The 61-element array, in Figure 15e, shows significant error toward the rear of the aircraft at the horizon where the corresponding SPL is minimal. This is possibly due to the interpolation scheme used to populate the surface of the hemisphere. The median error of the 61-element array is 0.06 (IQR 0.01-0.31) dB. Meanwhile, for the 73-element array, Figure 15f, the distribution differs from the reference array by six microphones beneath the vehicle. As can be seen, the difference produces negligible error indicating that the region below the vehicle is less sensitive to array resolution.

CONCLUSIONS

An acoustics research flight test was carried out by the Army/NASA in July of 2024. A novel snapshot array was deployed to capture acoustic emissions of the MD530F test vehicle. The design of the snapshot array was intended to capture all directivity angles simultaneously for a near instant in time. This is expected to be important for measuring acoustic directivity of VTOL UAM or FVL vehicles, which may possess multiple, independently controlled propulsors, and vehicle states that can not be assumed to be steady during flight.

One of the research goals was to determine adequate channel count for a snapshot array and so array resolution studies were conducted in post-processing. It was found that the higher channel count snapshot arrays, those based on the 61-element Lebedev distribution, were successful in qualitatively matching results from the traditional linear array method for both steady level and steady descending flight.

Generally, more microphones that can be used to estimate data at a point on the hemisphere result in both lower median errors and lower variation in errors. When considering the effects of directivity of emissions, LOO-CV can show what regions of the array are more sensitive. However, clustering microphones together can give a false sense of accuracy when evaluating with LOO-CV because parts of the region of interest are simply neglected. This was addressed using image comparison methods, such as absolute difference and the structural similarity index measures.

A limitation of all presented analysis methods is they assume that modified quadratic Shepard weighting on the surface is an adequate method of interpolation. Also, the choice of 30° as a radius of interpolation is arbitrary, although increasing this radius has not been shown to have a noticeable impact on results. Smaller RoI will not cover the entire surface of a hemisphere in the case of sparse microphone distributions.

A wealth of data was collected during this test. Moving on from analysis of the distributions themselves, this quasi-instantaneous data can be paired with vehicle state during maneuvers to correlate the loads on the vehicle with acoustic emissions.

REFERENCES

1. Conner, D. A., Burley, C. L., and Smith, C. D., "Flight Acoustic Testing and Data Acquisition for the Rotor Noise Model (RNM)," Proceedings of the 62nd Annual Forum of the American Helicopter Society, Phoenix, AZ, May 2006.

2. Watts, M. E., Greenwood, E., and Stephenson, J. H., "Measurement and Characterization of Helicopter Noise at Different Altitudes," Proceedings of the 72nd Annual Forum of the American Helicopter Society, West Palm Beach, FL, May 2016.

3. Pascioni, K. A., Greenwood, E., Watts, M. E., Smith, C. D., and Stephenson, J. H., "Medium-Sized Helicopter Noise Abatement Flight Test," Proceedings of the 76th

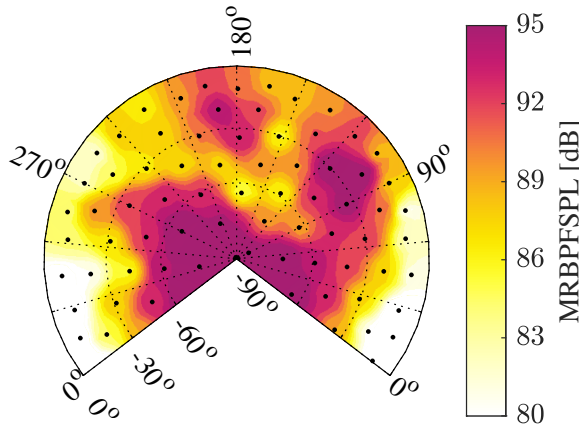

(a) 73-microphone array MRBPF SPL

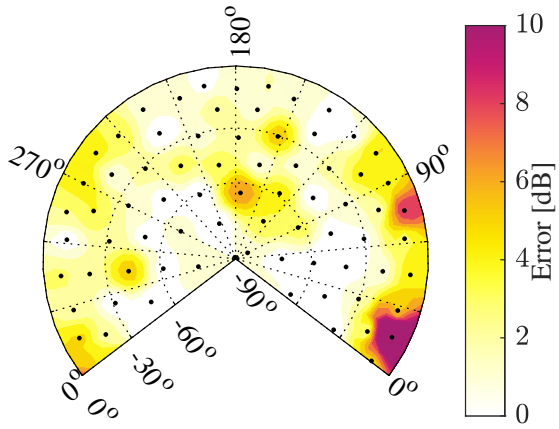

(b) 73-microphone array error for MRBPF noise

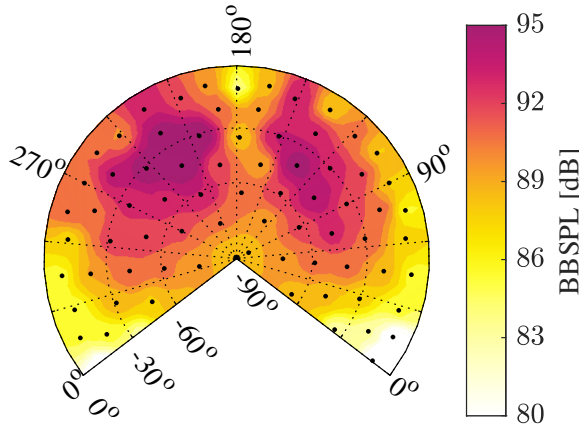

(c) 73-microphone array BB SPL

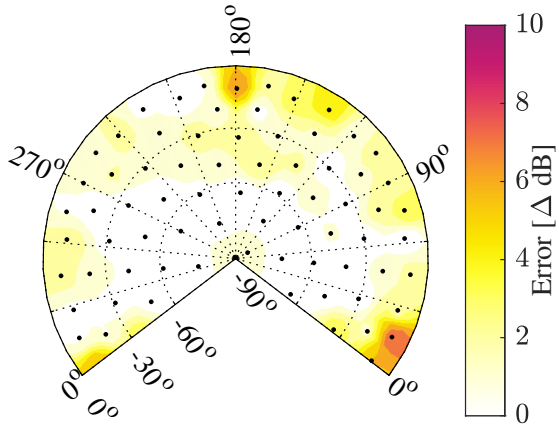

(d) 73-microphone array error for BB noise

Figure 13: Contour plots and associated errors from LOO-CV by frequency range for steady level flight at 75 kts.

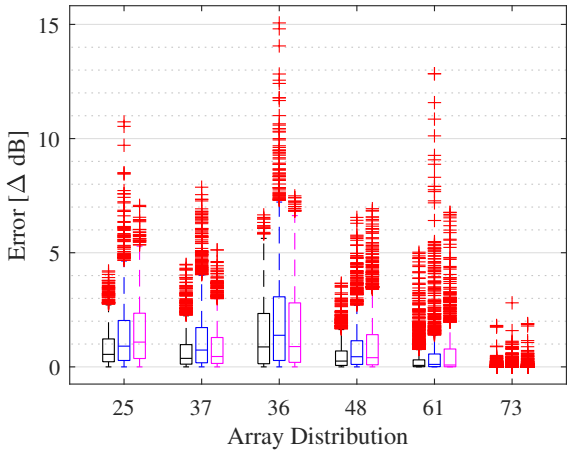

Figure 14: Absolute difference as a function of channel count and frequency distribution.

Annual Forum of the Vertical Flight Society, Virginia Beach, VA, October 2020.

4. Pascioni, K. A., Thai, A. D., and Bain, J. J., "Propeller Source Noise Separation from Flight Test Measurements of the Joby Aviation Aircraft," 30th AIAA/CEAS Aeroacoustics Conference, Rome, Italy, June 2024.

5. Spiegel, P., Buchholz, H., and Pott-Pollenske, M., "Highly Instrumented BO105 and EC135-FHS Aeroacoustic Flight Tests Including Maneuver Flights," Proceedings of the 61st Annual Forum of the American Helicopter Society, Grapevine, TX, June 2005.

6. Spiegel, P., Guntzer, F., Le Duc, A., and Buchholz, H., "Aeroacoustic Flight Test Data Analysis and Guidelines for Noise-Abatement-Procedure Design and Piloting," 34th European Rotorcraft Forum, Liverpool, UK., September 2008.

7. Stephenson, J. H. and Houston, M. L., "Rotorcraft Source Noise Characterization via Acoustic Snapshot Array: Development and Evaluation," *CEAS Aeronautical Journal*, Vol. 15, 2023, pp. 659–670.

8. Lebedev, V. I. and Laikov, D. N., "A Quadrature Formula for the Sphere of the 131st Algebraic Order of Accuracy," *Doklady Mathematics*, Vol. 59, (3), 1999, pp. 477–481.

9. Gelman, A., Carlin, J. B., Stern, H. S., Dunson, D. B., Vehtari, A., and Rubin, D. B., *Bayesian Data Analysis, Third Edition*, Chapman and Hall/CRC, 2013.

10. Wang, Z., Bovik, A., Sheikh, H., and Simoncelli, E., "Image quality assessment: from error visibility to structural similarity," *IEEE Transactions on Image Processing*, Vol. 13, (4), 2004, pp. 600–612.

11. Anderson, M. C., Stephenson, J. H., Zawodny, N. S., and Gee, K. L., "Characterizing the Effects of Two Ground-Based Outdoor Microphone Configurations," Proceedings of Meetings on Acoustics 178ASA, Vol. 39, 2019.

12. Stephenson, J. H., Pascioni, K. A., Houston, M. L., Stutz, C. M., and Martin, P. B., "Overview of a Comprehensive MD530F Acoustic Flight Test," Proceedings of the 81st Annual Forum of the Vertical Flight Society, Virginia Beach, VA, May 2025.

13. Stutz, C. M., Stephenson, J. H., Pascioni, K. A., and Houston, M. L., "Acoustic Assessment of an MD530F Helicopter in Maneuvering Flight," Proceedings of the 81st Annual Forum of the Vertical Flight Society, Virginia Beach, VA, May 2025.

14. Bass, H. E., Sutherland, L. C., Zuckerwar, A. J., Blackstock, D. T., and Hester, D., "Atmospheric absorption of sound: Further developments," *The Journal of the Acoustical Society of America*, Vol. 97, 1995, pp. 680–683.

15. Hubbard, H. H., "Aeroacoustics of Flight Vehicles: Theory and Practice. Volume One," NASA RP 1258, National Aeronautics and Space Administration, 1991.

16. Franke, R. and Nielson, G. M., "Scattered data interpolation and applications: A tutorial and survey," *Geometric Modeling: Methods and Applications*, 1991, pp. 131–160.

17. Page, J. A., Rapoza, A., Oberg, A., Hastings, A., Baker, G., and Shumway, M., "Advanced Acoustic Model Technical Reference and User Manual," Technical report, Volpe National Transportation Systems Center Cambridge MA, 2020.

18. Stephenson, J. H. and Pascioni, K. A., "Design of Experiments Development for Rotorcraft Acoustic Flight Testing," Proceedings of the 81st Annual Forum of the Vertical Flight Society, Virginia Beach, VA, May 2025.

19. Pascioni, K. A., Stutz, C. M., Houston, M. L., and Stephenson, J. H., "Phased Array Measurements of a Full-Scale Helicopter," Proceedings of the 81st Annual Forum of the Vertical Flight Society, Virginia Beach, VA, May 2025.

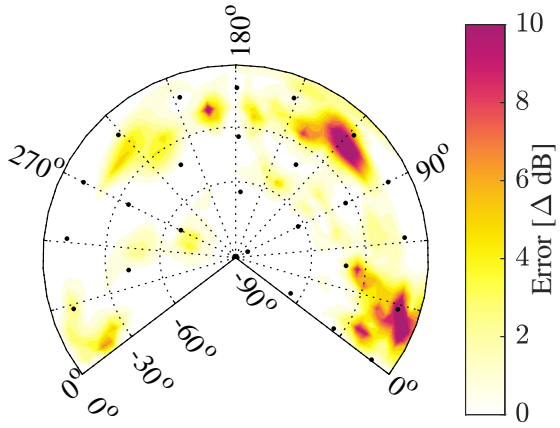

(a) 25-microphone array error for full frequency range

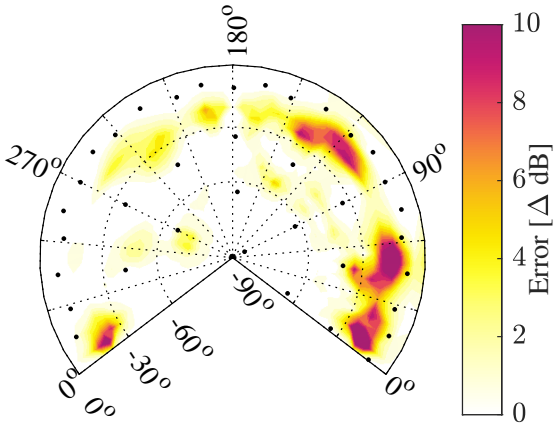

(b) 37-microphone array error for full frequency range

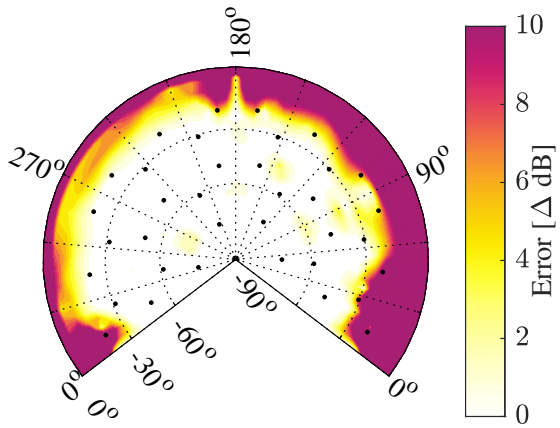

(c) 36-microphone array error for full frequency range

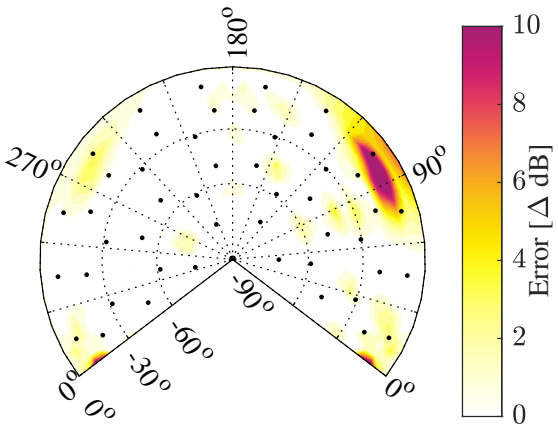

(d) 48-microphone array error for full frequency range

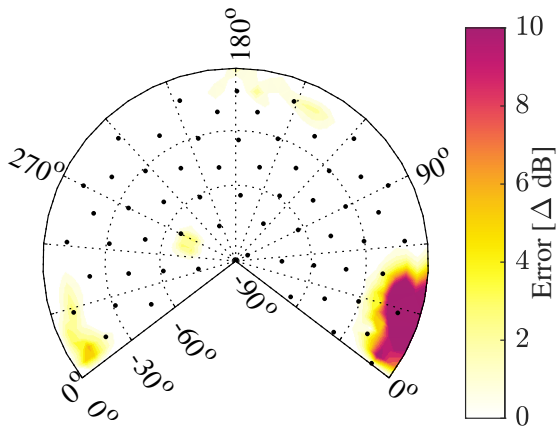

(e) 61-microphone array error for full frequency range

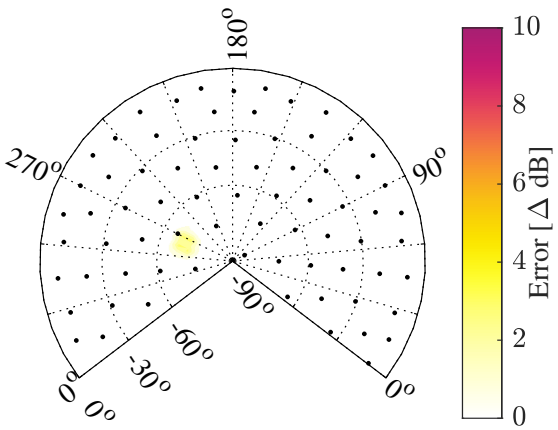

(f) 73-microphone array error for full frequency range

Figure 15: Errors using absolute difference relative to 79-microphone distribution for level flight at 75 kts.